

Facile and Efficient Atomic Hydrogenation Enabled Black TiO₂ with Enhanced Photo-Electrochemical Activity via a Favorably Low-Energy-Barrier Pathway

Xiaodan Wang, Leonhard Mayrhofer, Markus Hoefler, Sonia Estrade, Lluís Lopez-Conesa, Hao Zhou, Yuanjing Lin, Francesca Peiró, Zhiyong Fan,* Hao Shen,* Lothar Schaefer, Michael Moseler, Guenter Braeuer, and Andreas Waag*

Black TiO₂ has demonstrated a great potential for a variety of renewable energy technologies. However, its practical application is heavily hindered due to lack of efficient hydrogenation methods and a deeper understanding of hydrogenation mechanisms. Here, a simple and straightforward hot wire annealing (HWA) method is presented to prepare black TiO₂ (H-TiO₂) nanorods with enhanced photo-electrochemical (PEC) activity by means of atomic hydrogen [H]. Compared to conventional molecular hydrogen approaches, the HWA shows remarkable effectiveness without any detrimental side effects on the device structure, and simultaneously the photocurrent density of H-TiO₂ reaches 2.5 mA cm⁻² (at 1.23 V vs reversible hydrogen electrode (RHE)). Due to the controllable and reproducible [H] flux, the HWA can be developed as a standard hydrogenation method for black TiO₂. Meanwhile, the relationships between the wire temperatures, structural, optical, and photo-electrochemical properties are systematically investigated to verify the improved PEC activity. Furthermore, the density functional theory (DFT) study provides a comprehensive insight not only into the highly efficient mechanism of the HWA approach but also its favorably low-energy-barrier hydrogenation pathway. The findings will have a profound impact on the broad energy applications of H-TiO₂ and contribute to the fundamental understanding of its hydrogenation.


1. Introduction

Recently, black TiO₂ has shown significantly improved activity in the photocatalytic hydrogen generation due to its unique optical and electrical properties such as enhanced optical absorption and improved electron transport.^[1–3] Specifically, the black TiO₂ with disordered shell delivered superior properties to overcome the limitations of the large bandgap (rutile 3.0 eV; anatase 3.2 eV) and lower conductivity of pristine TiO₂,^[1] and improve visible light absorption, charge separation, and electron transport in the photo-electrochemical (PEC) process. Recently, Lü et al. fabricated TiO₂ homojunction films with an oxygen-deficient amorphous layer on top of a highly crystalline layer to simulate the similar structural and functional configuration of H-TiO₂ nanoparticles,^[4] and found that metallic conduction could be realized at the crystalline–amorphous homointerface via electronic interface reconstruction, which could explain the enhanced electron transport of black TiO₂.

Dr. X. D. Wang, Dr. M. Hoefler, Prof. H. Shen, Dr. L. Schaefer, Prof. G. Braeuer
Fraunhofer Institute for Surface Engineering and Thin Films
Bienroder Weg 54E, 38108 Braunschweig, Germany
E-mail: hshen678@126.com

Dr. X. D. Wang, H. Zhou, Prof. A. Waag
Institute for Semiconductor Technology
TU Braunschweig
Hans-Sommer-Strasse 66, 38106 Braunschweig, Germany
E-mail: a.waag@tu-bs.de

Dr. L. Mayrhofer, Prof. M. Moseler
Fraunhofer Institute for Mechanics of Materials IWM
Wöhlerstraße 11, 79108 Freiburg, Germany

 The ORCID identification number(s) for the author(s) of this article can be found under <https://doi.org/10.1002/aenm.201900725>.

DOI: 10.1002/aenm.201900725

Dr. S. Estrade, Dr. L. Lopez-Conesa, Prof. F. Peiró
Department d'Electrònica
Universitat de Barcelona
c/Martí Franquès 1, 08028 Barcelona, Spain

Dr. S. Estrade, Dr. L. Lopez-Conesa, Prof. F. Peiró
Institute of Nanoscience and Nanotechnology
Universitat de Barcelona (IN2UB)
c/Martí Franquès 1, 08028 Barcelona, Spain

Dr. Y. J. Lin, Prof. Z. Y. Fan
Department of Electronic and Computer Engineering
The Hong Kong University of Science and Technology
Clear Water Bay, Kowloon, Hong Kong S.A.R., China
E-mail: eezfan@ust.hk

Prof. H. Shen
School of Chemistry and Chemical Engineering
Jiangsu University
Xuefu Road 301, 212013 Zhenjiang, China

Wang et al. reported the visible-light photocatalytic and PEC properties of aluminum-reduced black TiO₂.^[5] The Al-reduced amorphous shell is proved to be responsible for the improved visible-light absorption. Zhang et al. revealed that the disordered shell trapped photogenerated holes and promoted the charge separation.^[6] Therefore, developing novel approaches to modify black TiO₂ with the disordered shell is critical to achieve enhanced PEC activity. Research efforts have been devoted to the development of hydrogenation approaches such as high-pressure hydrogenation,^[7] high-temperature hydrogen gas annealing,^[8] hydrogen thermal plasma annealing,^[9] most of which require rigid technical conditions such as high temperature or pressure, prolonged treatment time, high doses of molecular hydrogen H₂, or hydrogen plasma H⁺. For instance, Chen et al. reported the high-pressure hydrogenation of TiO₂ nanoparticles (20 bar H₂, 200 °C, 5 days).^[7] Wang et al. applied the high-temperature hydrogen annealing on the TiO₂ nanorods (1 bar H₂, 350–550 °C, 1 h).^[8] Wang et al. used the hydrogen plasma annealing on the TiO₂ nanoparticles (200 W, 500 °C, 4–8 h).^[9] To prepare black TiO₂ with disordered shell in more facile and cost-effective manners, solution-based reduction methods were also developed. However, due to surface defects and chemical residues, the achieved PEC activities of black TiO₂ are relatively poor with typical photocurrents lower than 2 mA cm⁻² (at 1.23 V vs reversible hydrogen electrode (RHE)).^[10–12] Very recently, Xu et al. used noble metallic Pd nanoparticles to dissociate H₂ to atomic [H] (spill-over effect) to prepare black TiO₂. The multi-step approach is efficient, but the achieved photocurrent density is limited to 2 mA cm⁻² (at 1.23 V vs RHE) possibly due to the chemical residues after Pd decoration.^[13] Additionally, the underlying mechanism of atomic hydrogenation is still unclear. A recent study also suggested that black TiO₂ with controllable crystal-deficient disordered shell attributed to the enhanced PEC activity.^[6] Currently, in order to achieve high PEC activity, the most commonly adopted hydrogenation approaches rely on molecular hydrogen gas or hydrogen plasma to treat TiO₂. However, the practical application of black TiO₂ is heavily hindered due to the extreme hydrogenation conditions like high temperature or pressure, as well as prolonged treatment time. Therefore, novel hydrogenation approaches with highly efficient, mild treatment conditions, and fabrication scalability are highly desirable to synthesize black TiO₂ with superior properties for practical PEC applications.

Furthermore, the interaction between hydrogen and TiO₂ is an important topic to understand the surface reaction of hydrogen on TiO₂^[14] and formation mechanism of disordered shell in black TiO₂.^[1–3] Several works were conducted by using a combination of scanning tunneling microscopy (STM)/atomic force microscopy (AFM) experiments and ab initio density functional theory (DFT) simulations.^[14–22] They studied the surface effects under very clean conditions and sub-monolayer coverage of atomic hydrogen. A comprehensive review of this complex topic is summarized in the Supporting Information. It is concluded that atomic hydrogen can be absorbed and diffused within the subsurface region of TiO₂^[14,18] or lead to the generation of oxygen vacancies via the desorption of H₂O.^[15,17] Till now, the surface modification mechanisms that determine the atomic or molecular hydrogenation processes leading to black TiO₂ are rarely studied.

In this work, we utilized hot wire annealing (HWA) to produce atomic hydrogen and successfully prepare H–TiO₂ nanorods on fluorine-doped tin oxide (F:SnO₂, FTO) conducting substrates at mild conditions; in addition, a high photocurrent density of 2.5 mA cm⁻² (at 1.23 V vs RHE) has been achieved. Systematic studies were carried out to reveal the influences of processing parameters, structural factors, and optical properties, so as to achieve the insight into the mechanism for enhanced PEC activity with atomic hydrogen treatment. Compared with conventional treatments by using molecular hydrogen gas and hydrogen plasma, the HWA method provides controllable active atomic hydrogen to prepare H–TiO₂ in large scales at relatively low substrate temperatures within short annealing time, while eliminating side actions from hydrogen ions and energetic neutrals, demonstrating itself as a promising and effective hydrogenation method to develop H–TiO₂ for applications such as photocatalytic hydrogen generation, rechargeable batteries, and supercapacitors.^[1–3] Moreover, to achieve a deeper understanding of the formation mechanisms of black TiO₂, DFT simulations were performed to compare different hydrogenation pathways via atomic hydrogen and molecular hydrogen approaches. The simulation results matched well with our experiments and revealed the thermodynamic stability of a high surface coverage of atomic hydrogen on the TiO₂ surface, which contributes to the efficient formation of disordered shell in black TiO₂.

2. Results and Discussion

2.1. Atomic Hydrogenation: HWA Approach

The approach of the present study applied highly active atomic hydrogen [H] simply generated by hot wires to treat TiO₂ nanorods.^[23] Figure 1a shows the typical configuration of the hot wire system for HWA of TiO₂ nanorods. A parallel arrangement of ten tungsten wires with 600 mm length and 0.53 mm diameter was equipped in a vacuum chamber. The distance between adjacent wires was 50 mm; thus, the distance between the first and the last wire was 450 mm, and the total activated area was 600 × 450 mm² (Figure 1a). The samples were treated at different wire temperatures (1600, 1700, and 1800 °C). The distance between the ten tungsten wires and the sample surface was 75 mm. During the treatments, the sample temperature increased to 245, 265, and 290 °C at wire temperatures $T_{\text{wire}} = 1600, 1700, \text{ and } 1800 \text{ °C}$, respectively (Table S1, Supporting Information). Since the generated atomic hydrogen depends on the wire dimension sizes, wire materials, and wire temperature and pressure, the flux rate of atomic hydrogen can be precisely controlled and adjusted by the wire temperature.^[23] The completed hydrogen treatments including all processing parameters (wire temperature, pressure, hydrogen flux, and time) were precisely controlled by a programmable recipe; therefore, reproducible hydrogenations on TiO₂ nanorods could be realized. Due to the simple technical configuration, the HWA is suitable for large-scaled hydrogenation of TiO₂ for a variety of practical energy applications. The advanced features of HWA can be listed as followed: i) the most effective hydrogenation method till now (low pressure: 1 Pa, low temperature:

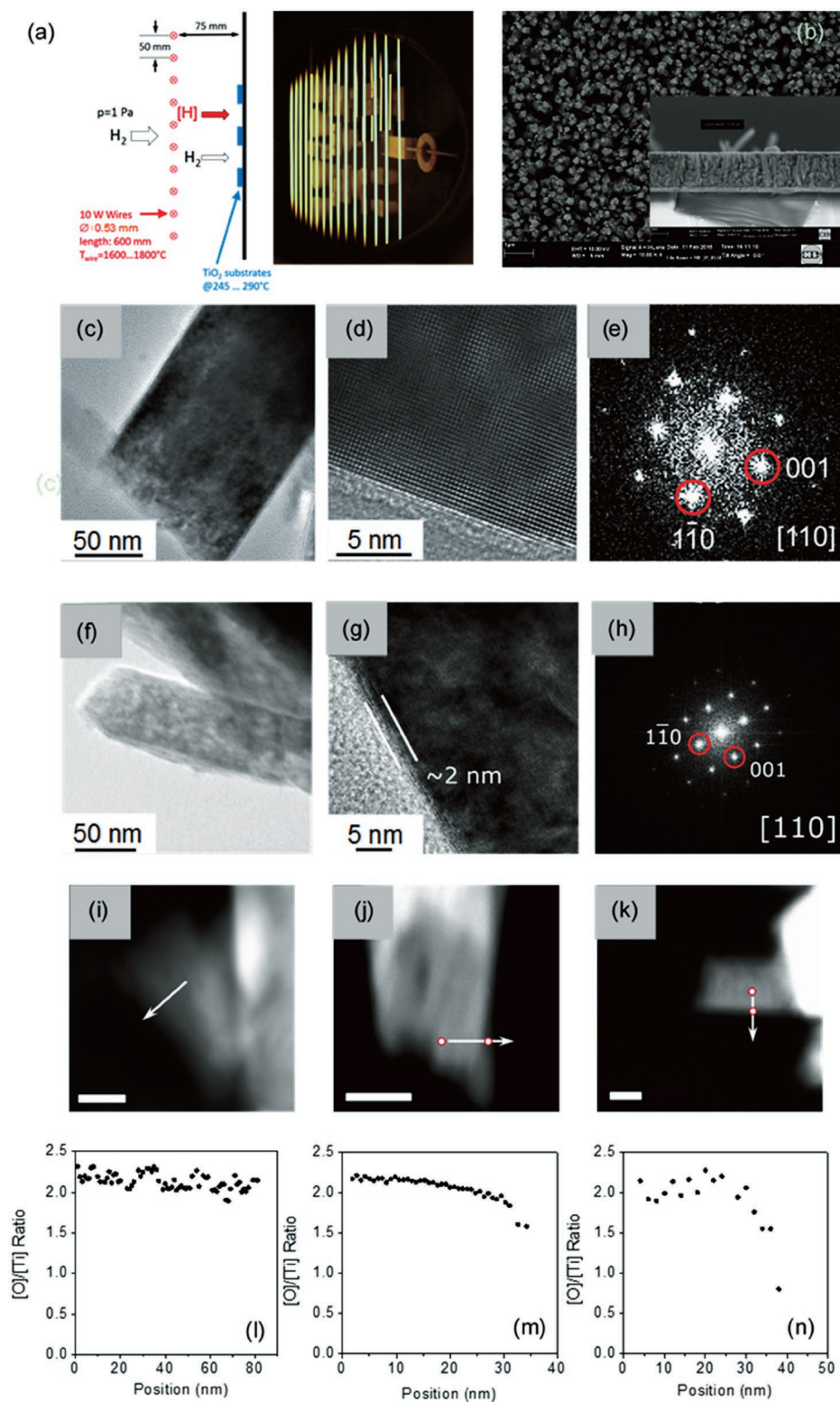


Figure 1. a) Schematic diagram of an HWA process (left) and photograph of a hot wire chemical vapor deposition (CVD) reactor equipped with vertically aligned tungsten wires (right). b) H-TiO₂ nanorods treated at T_{wire} = 1700 °C. Inset: cross-sectional SEM image of H-TiO₂ nanorods treated at T_{wire} = 1700 °C. TEM, HR-TEM images, and FFT patterns of c–e) pristine TiO₂ and f–h) H-TiO₂ nanorods treated at T_{wire} = 1700 °C. High angle annular dark field (HAADF)–scanning transmission electron microscopy (STEM) images for the i) pristine TiO₂ and H-TiO₂ treated at j) T_{wire} = 1700 °C, and k) 1800 °C, respectively; scale bar = 50 nm. The arrows correspond to the directions along which spatially localized EELS spectra were acquired. l–n) The corresponding [O]/[Ti] ratios obtained from the quantification of the acquired EELS spectra.

265 °C, and short time: 20 min); ii) one step and reproducible processing; iii) clean physical processing by using controllable and tunable flux rate of active atomic hydrogen to avoid the chemical residues; iv) general method for hydrogenation of inorganic metal oxides for broad applications;^[13] and v) large-scaled processing for practical applications. In comparison to inefficient molecular hydrogenation and multistep solution-based reduction approaches, HWA with controllable active atomic hydrogen can be developed to be a standard hydrogenation method for the fabrication of black TiO₂. The technical background of HWA is given in the Supporting Information.

2.2. The Influence of Wire Temperature on the Structural, Optical, and Photo-Electrochemical Properties

The core-shell structure of H-TiO₂ nanorods (Table S1, Supporting Information) was investigated by scanning electron microscopy (SEM) and high-resolution transmission electron microscopy (HR-TEM). The morphology of H-TiO₂ treated at a wire temperature of 1700 °C is similar to that of pristine TiO₂ (Figure 1b; Figure S1, Supporting Information). As indicated in the TEM and HR-TEM images (Figure 1c,d), the pristine TiO₂ nanorods are single crystalline, which was also confirmed by the fast Fourier transform (FFT) pattern presented in Figure 1e. The growth direction of the TiO₂ nanorods is [001] and the sidewalls are {110}. Figure 1f,g shows the TEM and HR-TEM images of H-TiO₂ nanorods treated at $T_{\text{wire}} = 1700$ °C. As shown in Figure 1g, the thickness of the disordered shell is around 2 nm. Figure S2 (Supporting Information) shows the TEM and HR-TEM images of H-TiO₂ nanorods treated at $T_{\text{wire}} = 1800$ °C. It is noted that the thickness of the disordered shell of H-TiO₂ at $T_{\text{wire}} = 1800$ °C is also around 2 nm while the intensity of its FFT pattern is weaker than that of H-TiO₂ treated at $T_{\text{wire}} = 1700$ °C (Figure 1h) indicating that more defective features are created in the case of H-TiO₂ at $T_{\text{wire}} = 1800$ °C. Figure 1i-k shows the line scan analysis in the high angle annular dark field (HAADF)-scanning transmission electron microscopy (STEM) images for the pristine TiO₂ and H-TiO₂ treated at $T_{\text{wire}} = 1700$ and 1800 °C, respectively. The line scan of [O]/[Ti] ratio (Figure 1l-n) was estimated from electron energy loss spectroscopy (EELS) spectra of Ti-L_{2,3} and O-K to study the compositional change before and after HWA. It is shown that the [O]/[Ti] ratio of pristine TiO₂ remains about 2 from the core to the surface of the TiO₂ nanorod whereas the [O]/[Ti] ratio of H-TiO₂ at $T_{\text{wire}} = 1700$ °C decreases gradually. The [O]/[Ti] ratio of H-TiO₂ treated at $T_{\text{wire}} = 1800$ °C decreases even more distinctly than that of H-TiO₂ at $T_{\text{wire}} = 1700$ °C. Abe et al. have measured the density of hydrogen atoms generated by heated tungsten wires in hydrogen atmosphere, which follows approximately an Arrhenius law with an activation energy of 2.53 eV.^[24] They set the pressure at 1.9 Pa, which is very close to the conditions we used for HWA treatments. From their data, the flux of hydrogen atoms can be estimated to increase from about 3.26×10^{16} atoms cm⁻² s⁻¹ at $T_{\text{wire}} = 1600$ °C to about 1.48×10^{17} atoms cm⁻² s⁻¹ at $T_{\text{wire}} = 1800$ °C which is an increase by almost five times (see the Supporting Information).

The optical absorption spectra of pristine TiO₂ and H-TiO₂ were recorded to study the modified optical absorption of

H-TiO₂. Figure S3a (Supporting Information) shows that the band edge of H-TiO₂ is redshifted with increased wire temperatures. In the visible range from 420 to 850 nm, the absorption of H-TiO₂ increases gradually with increased wire temperatures. Figure S3b (Supporting Information) shows the reflectance spectra of pristine TiO₂ and H-TiO₂ nanorods. It indicates a decreased reflectance ($\approx 50\%$) above the band edge of TiO₂ due to the light-trapping effect of 3D TiO₂ nanorod morphology. The Tauc plots in Figure S3c (Supporting Information) show that the band edge of H-TiO₂ is reduced to 2.9 eV in comparison to that of pristine TiO₂ (3.0 eV). A scheme for the conduction-valance band change between pristine TiO₂ and H-TiO₂ treated at $T_{\text{wire}} = 1600, 1700,$ and 1800 °C is provided in Figure S3d (Supporting Information).

To study the enhanced photo-electrochemical behavior of H-TiO₂ nanorods, the measurements of the photocurrent density versus potential (J - V) (Figure 2a) were performed in a three-electrode electrochemical system. The J - V curves of pristine TiO₂ and H-TiO₂ samples are compared to study the influence of wire temperature on the photocurrent density. Obviously, the photocurrent density increases after treatment at $T_{\text{wire}} = 1600$ °C, achieves its maximum value at $T_{\text{wire}} = 1700$ °C, and then decreases at $T_{\text{wire}} = 1800$ °C (Figure 2a). The photocurrent density of H-TiO₂ at $T_{\text{wire}} = 1700$ °C reaches ≈ 2.5 mA cm⁻² (at 1.23 V vs RHE) which is >3 times larger than that of pristine TiO₂.

Figure S4a (Supporting Information) shows the incident photon-to-current efficiency (IPCE) spectra of pristine TiO₂ and H-TiO₂ treated at $T_{\text{wire}} = 1600, 1700,$ and 1800 °C, respectively. In comparison to pristine TiO₂, the IPCE of H-TiO₂ shows the overall enhancement in the UV range from 300 to 420 nm. The IPCE of H-TiO₂ is $\geq 0.5\%$ in the range of $\lambda = 450$ -600 nm, whereas the IPCE of pristine TiO₂ is nearly zero (Figure S4b, Supporting Information). The band edge of H-TiO₂ at $T_{\text{wire}} = 1700$ °C shows the highest redshift whereas the band edge of H-TiO₂ at $T_{\text{wire}} = 1800$ °C is similar to that of H-TiO₂ at $T_{\text{wire}} = 1600$ °C but shows a small shoulder at 435 nm.

The influence of wire temperature on the conductivity of H-TiO₂ was studied by Mott-Schottky (M-S) measurement (Figure 2b). It is expected that the slope of H-TiO₂ decreases with increasing wire temperature indicating the increased donor density and conductivity according to the M-S equation (Equation (1))^[25]

$$N_d = \left(\frac{2}{\epsilon_0 \epsilon_r} \right) \left[\frac{d(1/C^2)}{dV} \right]^{-1} \quad (1)$$

Here N_d is the donor density, e_0 is the electron charge, ϵ_0 is the permittivity of vacuum, ϵ_r is the dielectric constant of TiO₂ nanorods, C is the capacitance, and V is the applied bias voltage. The calculated donor densities of H-TiO₂ are $(2.5 \pm 0.1) \times 10^{17}$ cm⁻³ (1600 °C), $(4.6 \pm 0.1) \times 10^{17}$ cm⁻³ (1700 °C), and $(2.1 \pm 0.2) \times 10^{18}$ cm⁻³ (1800 °C), which are higher than that of the pristine TiO₂ ($(1.5 \pm 0.1) \times 10^{17}$ cm⁻³) (Table S2, Supporting Information). It is evident that the H-TiO₂ samples become more conductive with increasing wire temperature. It correlates with the EELS results that increasing wire temperature results in higher amount of atomic hydrogen

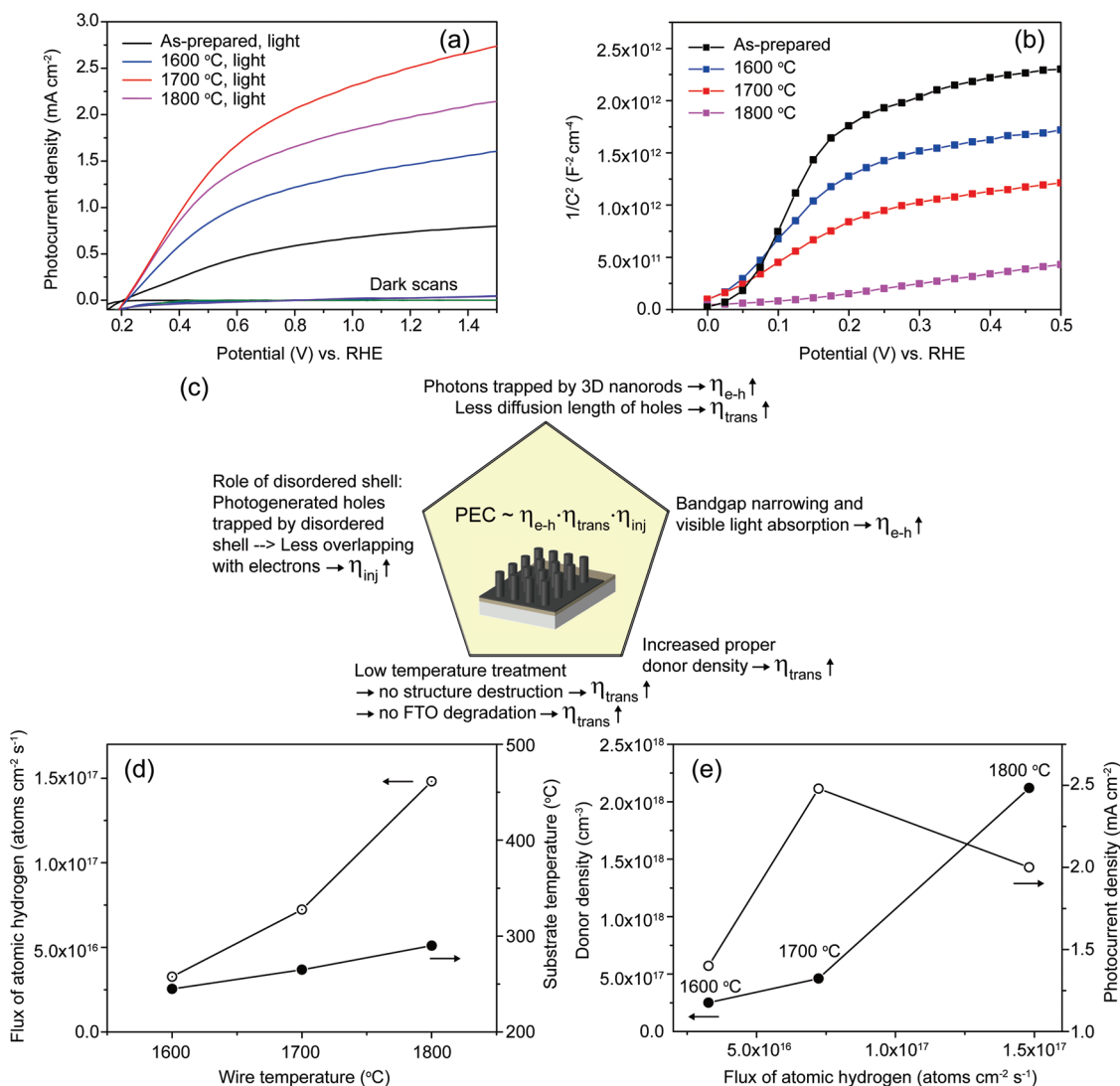


Figure 2. a) J - V curves of pristine TiO₂ and H-TiO₂ nanorods in 1 M KOH solution in the dark and under solar illumination. b) M - S plots of pristine TiO₂ and H-TiO₂ nanorods. c) A possible mechanism of enhanced photo-electrochemical behaviors of H-TiO₂ nanorods treated by atomic hydrogen. d) Flux of atomic hydrogen, substrate temperature versus wire temperature. e) Donor density, photocurrent density versus flux of atomic hydrogen.

leading to a stronger reduction of the surface of H-TiO₂ (Figure 1). Additionally, the flat band potentials (V_{fb}) of pristine TiO₂ and H-TiO₂ were determined by M - S plots (Figure 2b; Table S2, Supporting Information). The V_{fb} of H-TiO₂ treated at $T_{wire} = 1600$ °C is similar to that of pristine TiO₂; however, the V_{fb} was observed to decrease from 0.043 V (pristine TiO₂) to -0.005 V for the H-TiO₂ treated at $T_{wire} = 1700$ °C. The negative shift of V_{fb} at $T_{wire} = 1700$ °C could be attributed to the substantially increased donor density (Table S2, Supporting Information), which could consequently shift the Fermi level (E_F) of H-TiO₂ toward the conduction band (E_c). The V_{fb} was observed to increase from -0.005 V for the H-TiO₂ at $T_{wire} = 1700$ °C to 0.036 V for the H-TiO₂ at $T_{wire} = 1800$ °C. It could be due to the inhomogeneous defective structure of H-TiO₂ at $T_{wire} = 1800$ °C (Figure S2, Supporting Information).

Since no degradation issue of FTO electrode is observed in HWA (Tables S1 and S3, Supporting Information), the

relationships between wire temperature and structural, optical, and photo-electrochemical properties could be characterized in our study. Based on the X-ray diffraction (XRD) and SEM data (Figure S1, Supporting Information), the H-TiO₂ samples have the same rutile phase and similar morphology to pristine TiO₂. However, the marginal structural and composition changes of H-TiO₂ found in the HR-TEM and EELS analyses indicate that HWA affects only the topmost surface of TiO₂ without significant change of the bulk properties. The formation of a disordered shell on the surface of H-TiO₂ is observed in HR-TEM images (Figure 1g). The [O]/[Ti] ratios are different for the samples treated at $T_{wire} = 1700$ and 1800 °C, respectively (Figure 1m,n). The treatment of H-TiO₂ nanorods by HWA atomic hydrogen is mainly constricted to the surface compared to the treatment by molecular hydrogen. The thickness of the disordered shell (≈ 2 nm) of the H-TiO₂ by HWA is less than that of disordered shell (≈ 5 nm) from conventional molecular

hydrogen annealing.^[26] The penetration of atomic hydrogen seems to be restricted to the surface of TiO₂ nanorods because the reaction between TiO₂ and active atomic hydrogen will take place immediately once the atomic hydrogen reaches the surface of TiO₂, and subsurface diffusion of hydrogen is a slow process (see simulation). The optical absorption spectra show that HWA has a strong effect on the narrowing of the bandgap (from 3.0 to 2.9 eV) and the enhancement of visible light absorption (Figure S3, Supporting Information). The *J*-*V* curves show that the samples treated at *T*_{wire} = 1700 °C achieved the best PEC activity (2.5 mA cm⁻² at 1.23 V vs RHE) (Figure 2a). The IPCE curves support the relation between the wire temperature and photocurrent density (Figure S4, Supporting Information). The IPCE of H-TiO₂ for *T*_{wire} = 1700 °C shows the best redshift of band edge (bandgap narrowing) and the best improvement of visible photoactivity. Recently, two effective and practical hydrogenation approaches using either lithium reduction^[6] or Pd-catalyzed instant hydrogenation^[13] could achieve the maximum 2 mA cm⁻² photocurrent density at 1.23 V versus RHE. In comparison to the photocurrent density of these superior hydrogenation methods, our approach achieved 2.5 mA cm⁻² photocurrent density, 25% enhancement.

Figure 2c summarizes the possible mechanisms of enhanced PEC activity of H-TiO₂. i) The 3D nanorod morphology provides the large surface area and light-trapping ability to increase the efficiency of electron-hole (e-h) pair generation η_{e-h} .^[27-29] Additionally, in the nanorod arrays configuration, the photo-generated holes will choose the shortcut pathway via the radial direction.^[30-34] The diffusion length of photogenerated holes in 3D nanorods is much shorter than that of bulk materials. It means that the efficiency of hole transport η_{trans} is enhanced.^[35] ii) The bandgap narrowing and the increased visible absorption will increase the efficiency of e-h pair generation η_{e-h} .^[36] iii) The properly enhanced donor density will increase the efficiency of charge transport η_{trans} .^[4,8] iv) Due to the low-temperature treatment of HWA, the typical hydrogenation issues such as TiO₂ structure destruction and degradation of FTO will be avoided.^[8,37] The efficiency of charge transport η_{trans} will thus be enhanced due to fewer defects of H-TiO₂ and high conductivity of FTO current collector. v) Unlike an amorphous overlayer, the disordered shell is more like a crystal-deficient overlayer to overcome the efficiency of charge injection at TiO₂/electrolyte interface.^[6] The photogenerated holes are "trapped" in the disordered shell with less overlapping with delocalized electrons to increase the efficiency of charge injection.^[38]

Figure 2e shows that the H-TiO₂ treated at *T*_{wire} = 1700 °C achieved the best PEC activity whereas the photocurrent density of H-TiO₂ treated at higher wire temperature *T*_{wire} = 1800 °C decreased. It could be attributed to the following reasons:

i) *Improper Depletion Region Width:*

The donor densities of the H-TiO₂ nanorods were characterized via Mott-Schottky analysis. As shown in Figure 2b, the conductivity of H-TiO₂ increases with increased wire temperature. Table S2 (Supporting Information) shows the depletion region width (*W*) depending on the wire temperature. Since it is difficult to estimate the real active surface area of 3D H-TiO₂ nanorods, we followed the suggestion from Fabrega's work^[25] and assigned a donor density of 1.50×10^{17} cm⁻³ to the

pristine TiO₂. The equation to calculate the depletion region width is given as follows (Equation (2))

$$W = \sqrt{\frac{2\epsilon_0\epsilon_r|\phi_{sc}|}{e_0N_d}} \quad (2)$$

Here *N*_d is the donor density, *e*₀ is the electron charge, ϵ_0 is the permittivity of vacuum, ϵ_r is the dielectric constant of TiO₂ nanorods, $\phi_{sc} \equiv V - V_{fb}$ is the maximum potential drop on the depletion layer. It shows that the sample treated at *T*_{wire} = 1800 °C with the highest donor density has the lowest depletion region width (Table S2, Supporting Information). The narrow *W* leads to inefficient photoelectron-hole separation, which takes place locally near to the surface. The whole H-TiO₂ nanorods treated at *T*_{wire} = 1800 °C are not fully depleted in comparison to that of H-TiO₂ at *T*_{wire} = 1700 °C.

ii) *Improper Atomic Hydrogen Flux:*

Abe et al. measured the density of atomic hydrogen generated from the tungsten wires.^[24] Since we used a similar condition, the flux of atomic hydrogen at *T*_{wire} = 1600, 1700, and 1800 °C can be estimated (Figures S5 and S6, Supporting Information). Figure S6 (Supporting Information) shows that atomic hydrogen flux increases exponentially with the wire temperature.^[39] To understand the relationship between the processing parameters and the PEC properties, we plotted the calculated values of atomic hydrogen flux for the different wire temperatures against the donor density and the photocurrent density, respectively. The flux of atomic hydrogen increases exponentially with increased wire temperature (Figure 2d). Figure 2e shows that the donor density also increases exponentially with increased atomic hydrogen flux whereas the photocurrent density reaches the maximum at *T*_{wire} = 1700 °C and decreases at *T*_{wire} = 1800 °C. The high doses of atomic hydrogen flux at higher wire temperatures could result in higher defect concentrations and lower PEC activity.

The higher defects in H-TiO₂ at higher wire temperatures can be confirmed by TEM and EELS analyses. TEM results show that the thickness of the disordered shell of H-TiO₂ treated at *T*_{wire} = 1800 °C is similar to that of H-TiO₂ treated at *T*_{wire} = 1700 °C. However, a > 2 times flux of atomic hydrogen is dosed in H-TiO₂ treated at *T*_{wire} = 1800 °C than that of H-TiO₂ treated at *T*_{wire} = 1700 °C. In the case of 1800 °C wire temperature, the intensive hydrogenation together with the enhanced substrate temperature could create more oxygen vacancies, which is supported by EELS results (Figure 1n). The [O]/[Ti] ratio at the surface of H-TiO₂ treated at *T*_{wire} = 1800 °C decreases below 1. The HR-TEM image of H-TiO₂ treated at *T*_{wire} = 1800 °C (Figure S2, Supporting Information) shows a homogeneous structure through the TiO₂ nanorods; no evidence of agglomeration of Ti atoms to metallic Ti nanoparticles is found in any nanorods during the multiple observation sessions, either already present in the samples or induced by the electron beam irradiation. X-ray photoelectron spectroscopy (XPS) results show that Ti-H peak (456.5 eV) instead of metallic Ti (453.8 eV) is observed in the sample treated at *T*_{wire} = 1800 °C (Figure S7, Supporting Information). The formation of surface Ti-H bonds in H-TiO₂ would occur at the expense of surface Ti-OH bonds. More oxygen vacancies are formed via

excess [H]. Oxygen vacancies are occupied by [H] to form H_O defects which could be detrimental to the PEC activity (see the Supporting Information). It is evident that the HWA treatment of H-TiO₂ at $T_{\text{wire}} = 1800$ °C is possibly too strong so that the structure of the H-TiO₂ nanorods is negatively affected.

To understand the defect changes of H-TiO₂ nanorods after the HWA treatment, the EELS spectra of H-TiO₂ treated at $T_{\text{wire}} = 1700$ and 1800 °C at core and shell positions are compared (Figure S8, Supporting Information). The Ti-L₂₃ edge of H-TiO₂ “shell” treated at $T_{\text{wire}} = 1700$ °C shifts toward lower energy in comparison to that of the H-TiO₂ “core,” indicating the generation of Ti³⁺ species.^[13] It is noted that the Ti-L₂₃ edge of H-TiO₂ “shell” treated at $T_{\text{wire}} = 1800$ °C shifts also toward low energy in comparison to that of the H-TiO₂ “core,” but the shift is lower than that of H-TiO₂ treated at $T_{\text{wire}} = 1700$ °C, indicating lower concentration of Ti³⁺ species than that of H-TiO₂ treated at $T_{\text{wire}} = 1700$ °C. It is evident that the atomic hydrogen flux will also influence the concentration of Ti³⁺ species in the disordered shell and thus the PEC activity. Table S4 (Supporting Information) shows the possible charge-transfer model of H-TiO₂ samples treated at different wire temperatures. It is clear that H-TiO₂ treated at $T_{\text{wire}} = 1700$ °C achieves the best PEC activity due to more suppression of e-h recombination.

2.3. DFT Study on the Formation Mechanism of Atomic Hydrogenation

To understand the formation mechanism of black TiO₂ by efficient atomic hydrogenation, here we used DFT simulations to study the interaction between [H] and rutile TiO₂ (110) “on a microscopic level” in comparison to that of molecular H₂ and TiO₂ taking into account thermodynamic aspects and investigating the possibility of subsurface hydrogen diffusion in case of an atomic hydrogen environment. The hydrogenation process is discussed in the following three steps: a) hydroxylation of the TiO₂ (110) surface by hydrogen adsorption; b) subsurface diffusion of hydrogen; c) subsurface hydrogenation. Since the interaction between hydrogen and TiO₂ is a complex topic, a state of the art is summarized (see the Supporting Information).

2.3.1. Hydroxylation of the TiO₂ (110) Surface by Hydrogen Adsorption

Similar to the work of Kowalski et al.,^[14] we determined the hydrogen adsorption energy for surfaces with different hydrogen coverages. We employed periodically repeated slab models with 2 × 4 surface unit cells and 6 O-Ti-O trilayers where the two layers at the bottom were fixed. Here we investigated hydrogen coverages of 1/4, 1, and 9/8 ML and determined the corresponding relative Gibbs free energies as a function of the hydrogen chemical potential μ_{H} which is given with respect to the DFT ground state energy of an isolated hydrogen atom μ_{H}^0 (Figure 3). For the coverages of 1/4 and 1 ML, the hydrogen atoms are assumed to occupy the twofold coordinated O_{2c} surface ions (Figure S9, Supporting Information).^[14] In case of the 9/8 ML coverage, the additional H atom in the simulation

box energetically favors the occupation of a threefold coordinated O_{3c} surface site, Figure 3a–c. At the chemical potential of atomic hydrogen corresponding to the experimental conditions of 0.01 Pa partial atomic hydrogen pressure and a temperature of 265 °C or 538 K, the surface with the highest investigated hydrogen coverage of 9/8 ML is thermodynamically most stable; see Figure 3d. Higher hydrogen surface coverages might be even more favorable under these conditions but were not simulated here.

As can also be seen from Figure 3d, at a lower chemical potential of $\mu_{\text{H}} - \mu_{\text{H}}^0 = -2.44$ eV corresponding to a molecular hydrogen atmosphere, the 1/4 ML hydrogen coverage becomes thermodynamically more favorable. This crossover corresponds to a molecular hydrogen pressure of 70 bar at a typical molecular hydrogen treatment temperature of 400 °C. For sub-monolayer coverages > 1/4 ML (not investigated here), this crossover will take place at higher chemical potentials corresponding to even higher pressures of molecular hydrogen as shown by the simulations of Kowalski et al.^[14] In general, the molecular hydrogen treatment processes will result in sub-monolayer hydrogen coverages. In case of an atomic hydrogen treatment with higher chemical potential, the desorption of H₂ molecules cannot be excluded. The overall hydrogen coverage will reach a stationary state depending on the adsorption and desorption kinetics, which are investigated in the following. In the case of atomic hydrogen, the hydrogen adsorption shows very low or no energy barriers. The atomic hydrogen adsorption at an O_{2c} site to change the coverage from 7/8 to 1 ML yields a barrier of 0.02 eV (not shown). Furthermore, for the 1 ML covered surface, our simulations predict barriers of 0.08 and 0.12 eV for hydrogen adsorption at an O_{3c} surface site and at an O_{2c} surface site, respectively. The resulting configurations are denoted as HO_{3c} and H₂O_{2c} in Figure 3e. In the latter case, a chemisorbed H₂O molecule is obtained. The adsorbed H₂O molecule, however, shows an almost vanishing energy barrier to dissociate and hydroxylate an adjacent O_{3c} surface site of the HO_{3c} state. Alternatively, the H₂O molecule could also desorb from the surface, thereby creating an oxygen vacancy. Disregarding temperature, this process is endothermic. Yet, at higher temperatures H₂O desorption is mainly driven by entropy and the desorption barrier can be approximated by the free energy of the desorbed water molecule.^[17] Thus, at sufficiently high temperatures, H₂O desorption will compete with the dissociation reaction which leads to the formation of the HO_{3c} surface configuration. According to the work reported by Du et al.,^[17] the H₂O desorption becomes exothermic at temperatures between 500 and 600 K. We note that these values are very close to the substrate temperatures during our hydrogenation process which range from 518 to 563 K for the different wire temperatures from 1600 to 1800 °C.

In addition to O_{2c} and O_{3c} surface sites, atomic hydrogen can also be adsorbed at a fivefold coordinated Ti_{5c} titanium surface ion. The corresponding configuration is denoted as HTi_{5c} in Figure 3e. This process has no energy barrier since the energy is monotonically decreasing along the adsorption path such that the occupation of Ti_{5c} surfaces sites by hydrogen is a highly likely process. A transition from the HTi_{5c} configuration to the energetically more stable HO_{3c} configuration is, however, kinetically suppressed by an energy barrier of 1.53 eV.

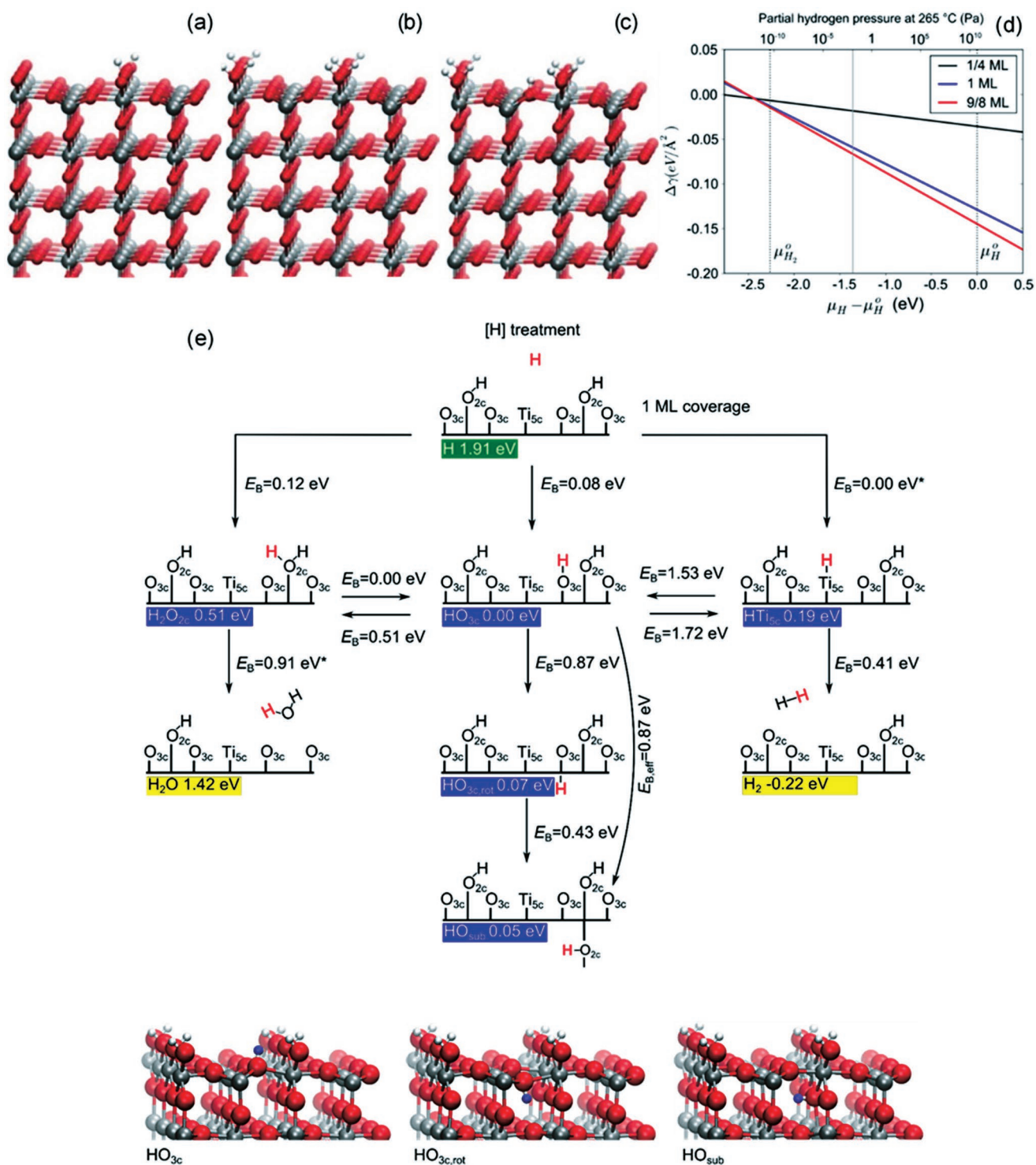


Figure 3. a–c) Atomistic structures of TiO₂ (110) with 1/4, 1, and 9/8 ML surface coverages. d) Gibbs free energy of the different surface coverages versus hydrogen chemical potential and partial pressure of atomic hydrogen at $T = 265$ °C. The hydrogen chemical potential μ_H is given with respect to the DFT ground state energy of a single hydrogen atom μ_H^0 . The DFT ground state energies of single hydrogen atoms (μ_H^0) and molecules ($\mu_{H_2}^0$) are indicated by dotted vertical lines. The chemical potential corresponding to the partial atomic hydrogen pressure of 0.01 Pa is shown by a solid vertical line. e) Hydrogenation pathways of atomic hydrogen in contact with the (110) rutile surface with an initial hydrogen coverage of 1 ML with corresponding energy barriers E_B . The surface configuration labeled by a green field has a 1 ML hydrogen coverage corresponding to eight hydrogen atoms per surface unit cell in our DFT simulations. Surface states with 9/8 ML coverage or nine hydrogen surface atoms per unit cell are indicated by blue fields and yellow fields are used to indicate a 7/8 ML hydrogen coverage. The DFT ground state energies of the different configurations are given with respect to the lowest-energy configuration HO_{3c} of the surface with 9/8 ML coverage.

In the next step, we discuss H_2 desorption from the TiO_2 rutile (110) surface with 9/8 ML hydrogen coverage in order to investigate whether high hydrogen coverages are unstable against fast H_2 desorption. From previous DFT studies using the Perdew–Burke–Ernzerhof (PBE) functional, the formation and desorption of H_2 molecules from adjacent hydroxylated O_{2c} sites of the (110) rutile surface with sub-monolayer hydrogen coverage was found to be suppressed due to high-activation barriers of around 2 eV.^[14,15] A similar value of 2.5 eV was obtained for the H_2 desorption from O_{2c} sites of the anatase (101) surface using the PBE0 hybrid functional.^[16] Using the PBE + U approach, we obtained a similar barrier of 1.72 eV for H_2 desorption from a hydroxylated O_{3c}/O_{2c} surface site pair of the most stable surface configuration HO_{3c} with 9/8 ML hydrogen coverage. Here, instead of a direct desorption, the process via the intermediate occupation of a Ti_{5c} surface site (HTi_{5c} in Figure 3e) is favored in agreement with the work of Wang and Fan.^[15] Due to the large energy barrier, H_2 desorption will be kinetically suppressed from the energetically most stable HO_{3c} configuration compared to the fast adsorption kinetics of atomic hydrogen. Interestingly, H_2 desorption from the configuration HTi_{5c} with hydroxylated O_{2c}/Ti_{5c} surface site pairs shows a considerably lower desorption barrier of 0.41 eV and hence hydroxylated Ti_{5c} sites which have vanishing adsorption barriers for atomic hydrogen can easily release H_2 during the atomic hydrogenation process.

In total, our simulations indicate that the adsorption of atomic hydrogen is a very fast process compared to H_2 desorption for all of the three different surface site species O_{2c} , O_{3c} , and Ti_{5c} , such that under the condition of an atomic hydrogen environment, a high hydrogen coverage of the (110) rutile surface can be expected. Of importance is that at high surface hydrogen coverages beyond 1 ML, the occupation of O_{3c} sites can be expected, since this is energetically the most favorable configuration, and H_2 desorption from hydroxylated O_{3c}/O_{2c} pairs is kinetically suppressed. For comparison and to identify main differences between the atomic and molecular hydrogenation approaches, we have additionally investigated the hydroxylation of a (110) rutile surface by molecular hydrogen (see the Supporting Information). The main results are that thermodynamically only sub-monolayer hydrogen coverages of the (110) surface are stable and that the dissociative adsorption of molecular hydrogen at the favored O_{2c} surface sites is kinetically suppressed due to high energy barriers, whereas the formation of oxygen vacancies via the desorption of H_2O can be expected at high-enough temperatures (Figure S10, Supporting Information).

2.3.2. Subsurface Diffusion of Hydrogen

In the work by Yin et al.^[18] where high hydrogen surface coverages were obtained after a single exposure of a rutile (110) surface to atomic hydrogen, only very weak H_2 and H_2O desorption was observed, although the surface hydroxylation degree decreased gradually with increasing surface temperature. It was concluded that the hydrogen diffused into the subsurface region. However, the subsurface diffusion turned out to be a controversial topic, since DFT simulations showed that the hydrogen pathway from the energetically favored O_{2c} surface

sites at sub-monolayer hydrogen coverage to the first subsurface layer has a rather high energy barrier of more than 1.5 eV and hence it is a very slow process at moderate temperatures.^[19,20] On the other hand, the subsurface diffusion starting from the O_{3c} surface sites has a considerably lower energy barrier of around 1 eV or below.^[14,18] As we have shown above in the case of atomic hydrogen treatment high surface coverages beyond 1 ML resulting in the formation of hydroxyl groups at O_{3c} sites can be expected. From our simulations we identified an effective barrier of 0.87 eV for the diffusion of hydrogen from the lowest-energy configuration HO_{3c} of the 9/8 ML covered surface with the occupied O_{3c} surface sites to the first subsurface layer (Figure 3e) in good agreement with the calculations at lower surface coverages.^[14,18] Hence, subsurface diffusion from the HO_{3c} state with 9/8 ML coverage has indeed a lower energy barrier than the corresponding barrier for H_2 desorption. At sufficiently low temperatures, hydrogen subsurface diffusion will also dominate over H_2O desorption which is purely driven by entropy. Additionally, it was shown that surface oxygen vacancies suppress H_2O desorption^[15] such that at sufficiently high concentrations of surface oxygen vacancies, hydrogen subsurface diffusion will also likely dominate over H_2O desorption.

In summary, our simulations indicate that as a result of O_{3c} surface sites occupied by hydrogen the subsequent subsurface hydrogenation can be expected in case of atomic hydrogen treatment depending on the substrate temperature. However, in case of a molecular hydrogen treatment, in general only sub-monolayer hydroxylation degrees are obtained and the occupation of O_{3c} sites is thermodynamically not favorable. Hence subsurface diffusion $O_{2c} \rightarrow O_{sub}$ is kinetically suppressed in case of a molecular hydrogen treatment (Figure S10, Supporting Information).

2.3.3. Subsurface Hydrogenation

Our simulations of surface hydroxylation and hydrogen diffusion indicate that in an environment of atomic hydrogen atmosphere, the subsurface diffusion is a viable hydrogenation route. In the next step, we investigated if the absorption of hydrogen in the subsurface region is thermodynamically possible with respect to the chemical potential of atomic hydrogen and whether we see a dependence of the absorption energetics on the concentration of absorbed hydrogen. To answer this question, slab models with 2×3 surface unit cells and 4 O–Ti–O trilayers were set up, and all twofold coordinated oxygen surface ions at the top and bottom surface were saturated with H from the beginning corresponding to a 1 ML coverage. Then the hydrogen concentration of the TiO_2 slabs was successively increased by randomly inserting H ions into the TiO_2 slabs. The investigated compositions of the simulation box were $Ti_{48}O_{96}H_{12+n \cdot 6}$, $n = 0, 1, \dots, 11, 12$ corresponding to subsurface hydrogen concentrations of 0–1.9 wt%. For each composition, eight different random samples were generated and relaxed. It was asserted that during the relaxation process, no H_2 molecules were formed but that all hydrogen atoms were chemically bonded to the TiO_2 lattice. In Figure 4c, the DFT cohesive energy evolution is shown for the different compositions. Interestingly, a linear dependence of the cohesive energy on the H concentration is found up to the

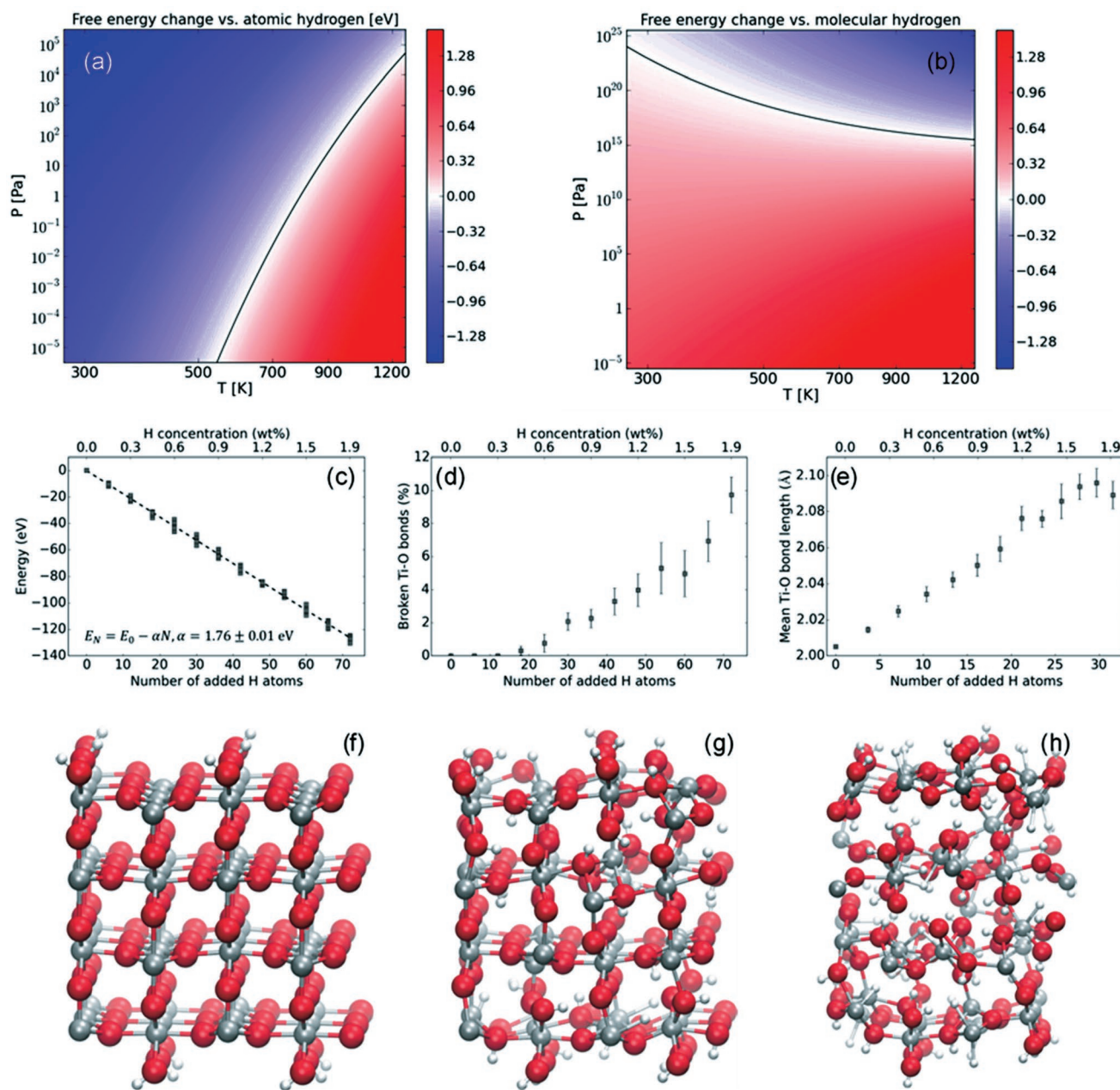


Figure 4. a) Adsorption free energy change for H incorporation in TiO₂ lattice as a function of temperature and pressure. Blue area corresponds to negative free energy changes and thus to conditions where H absorption is thermodynamically favorable. The line of zero free energy change is shown as a black line. b) Like panel (a), but with molecular hydrogen as the reference. c) DFT cohesive energy with respect to atomic hydrogen as reference versus number N of randomly added hydrogen atoms in TiO₂ slab models with composition Ti₄₈O₉₆H_{12+N}. The corresponding weight percentage of additional hydrogen is also shown. A linear regression yields an average energy gain of 1.76 ± 0.01 eV for uptake of one hydrogen atom. d) Percentage of broken Ti–O bonds as a function of the number of added H atoms per supercell and the corresponding H concentration in wt%. e) Mean Ti–O bond lengths as a function of the number of added H atoms per supercell and the corresponding H concentration in wt%. Error bars in panels (d) and (e) indicate the standard deviation of the eight random samples per system composition. f–h) Examples of relaxed TiO₂ model slabs with compositions Ti₄₈O₉₆H_{12+N}, $N = 0, 36,$ and 72 .

highest investigated concentrations. A linear regression yields an absorption energy $E_{\text{H,ab}} = -1.76 \pm 0.01$ eV per hydrogen atom where $E_{\text{H,ab}}$ is given with respect to atomic hydrogen, $E_{\text{H,ab}} = E_{\text{Ti}_{48}\text{O}_{96}\text{H}_{12+N}} - (E_{\text{Ti}_{48}\text{O}_{96}\text{H}_{12}}^{\text{ref}} + N_{\text{H}} \cdot E_{\text{H,atomic}})$. Negative values indicate that the H absorption is stable with respect to atomic H. Using molecular hydrogen as a reference, the absorption energy

becomes positive $E_{\text{H,ab}}^{\text{mol}} = +0.50$ eV meaning that the incorporation of H into the TiO₂ subsurface region is energetically not favorable in the presence of a molecular hydrogen environment. At elevated temperatures and low pressures, H absorption is less favorable due to thermodynamic effects; see Figure 4. From a thermodynamic point of view, the hydrogen incorporation

into the TiO₂ lattice is favorable if the surface is in contact with atomic hydrogen under the experimental conditions of substrate temperatures of around 265 °C (538 K) and an atomic hydrogen pressure of 0.01 Pa, but on the other hand, it is not stable with respect to H₂ desorption; see Figure 4a,b. However, the H₂ desorption is, kinetically, strongly suppressed at moderate temperatures as shown above. We note that the steady-state absorption concentration of H in the subsurface region of TiO₂ during the hydrogen treatment will be determined by the kinetics of adsorption and diffusion of atomic hydrogen on the one hand and the desorption kinetics of H₂ or surface H₂O on the other hand. Moreover, as a structural analysis of the simulated TiO₂ slabs shows, see the following sections, at high concentrations of absorbed H, the TiO₂ lattice becomes distorted by the breaking and elongation of Ti–O bonds which might lead in turn to altered diffusion barriers and kinetics. A more detailed investigation of the surface hydrogenation of TiO₂ including the effect of structural changes, temperature, hydrogen coverage, and oxygen vacancy concentration will give additional insights into the hydrogenation process using atomic hydrogen, but is beyond the scope of the present work.

Thus, from the thermodynamic point of view, atomic hydrogen can easily be incorporated into the subsurface region at the substrate temperatures and hydrogen pressures of our experiments whereas with molecular hydrogen as reference, the incorporation of hydrogen in the TiO₂ lattice seems not to be feasible, unless extremely high molecular hydrogen pressures beyond 10¹⁵ Pa are applied in the investigated temperature range between 273 and 1273 K (Figure 4b).

In order to understand if a high concentration of atomic hydrogen in the TiO₂ subsurface region can lead to structural lattice disorder, the structure of the hydrogenated TiO₂ slabs was analyzed as a function of hydrogen content. Structural changes in TiO₂ require the breaking or weakening of Ti–O bonds.^[18] Our structural analysis shows that our relaxed configurations with randomly added H ions are indeed prone to the breaking of Ti–O bonds with increasing hydrogen content (Figure 4d). Moreover, we also find that the remaining Ti–O bonds are elongated with respect to the hydrogen-free reference system; see Figure 4e. As cutoff for the Ti–O bonds, we have chosen a value of 2.5 Å which is well above the value of the mean Ti–O bond length of 2.0 Å of the reference slab model.

2.4. The Interaction Between [H] and TiO₂ at Different Wire Temperatures and Its Effect on the Photo-Electrochemical Activity

2.4.1. The Interaction between [H] and TiO₂ at Different Wire Temperatures Based on EELS, XPS, and DFT Results

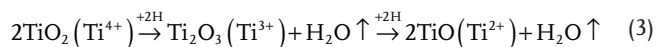
H–TiO₂ Samples at T_{wire} = 1600 °C: H incorporated in disordered TiO₂ lattice, subsurface diffusion of H to form OH groups in the subsurface area is the main hydrogenation process. This leads to Ti³⁺ ions (localized polarons) and hence to increased charge carrier density compared to the pristine sample.

H–TiO₂ Samples at T_{wire} = 1700 °C: H incorporated in disordered TiO₂ lattice is the main hydrogenation process. Ti³⁺ ions

are formed due to H doping and Ti–OH formation. Due to the higher H flux, the Ti³⁺ concentration is larger than that in the 1600 °C sample. Additionally, H₂O desorption and the simultaneous formation of oxygen vacancies takes place at low rates due to low substrate temperature and relatively low [H] flux.

H–TiO₂ Samples at T_{wire} = 1800 °C: H incorporated in disordered TiO₂ lattice to form Ti–OH. More oxygen vacancies (Vo) are formed due to excess [H] (strong reduction) and local surface heating via the recombination of H pairs. Oxygen vacancies are occupied by H to form H_O defects.

Figure S6 (Supporting Information) shows that the flux of atomic hydrogen increases exponentially (not linearly) with increasing wire temperature. The flux of [H] at T_{wire} = 1800 °C is two times higher than that at T_{wire} = 1700 °C. It is possible that more oxygen vacancies are formed on the surface of sample treated at T_{wire} = 1800 °C by [H] resulting in [O]/[Ti] ratio below 1 at the surface of H–TiO₂. Figure 1m shows gradual small change of [O]/[Ti] in the 1700 °C sample whereas a dynamically big change of [O]/[Ti] (below 1 near to surface) in the 1800 °C sample is observed in Figure 1n indicating the formation of oxygen vacancies and destruction in the 1800 °C sample. Additionally, the FFT patterns of the 1800 °C sample (Figure S2c, Supporting Information) are more diffuse than that of the 1700 °C sample (Figure 1h) indicating the highly defective structures in the 1800 °C sample. Due to strong H reduction on the sample treated at T_{wire} = 1800 °C, the concentration of Ti³⁺ decreases due to the destructive and unstable chemical surrounding, such that the following reaction Ti⁴⁺ → Ti³⁺ → Ti²⁺ will take place



In total, the concentration of Ti³⁺ species in H–TiO₂ treated at T_{wire} = 1800 °C is lower than that of H–TiO₂ treated at T_{wire} = 1700 °C.

2.4.2. The Relation between [H], Wire Temperature, Ti Species, Defects, and PEC Activity

It is evident that the Ti³⁺ concentration increases with increasing the wire temperature from 1600 to 1700 °C and decreases with further increasing the wire temperature to 1800 °C (Ti³⁺(1600 °C) < Ti³⁺(1700 °C) > Ti³⁺(1800 °C)). Since Ti³⁺ is responsible for the bandgap narrowing and enhanced visible-light absorption,^[9] it shows the similar tendency in our optical absorption spectra (Figure S3, Supporting Information). Figure S11 (Supporting Information) shows the typical formation of occupied Ti³⁺ midgap in the bandgap to promote the visible-light absorption and enhance the visible-light-driven PEC activity. Higher Ti³⁺ concentration in the H–TiO₂ sample treated at T_{wire} = 1700 °C results in narrower bandgap (2.92 eV) and better visible-light absorption to increase the efficiency of e–h pair generation and enhance the photocurrent density (2.5 mA cm^{–2} at 1.23 V vs RHE). Due to the strong hydrogenation in the H–TiO₂ sample treated at T_{wire} = 1800 °C, the formed defective structure will increase the e–h recombination rate k_r and decrease the photocurrent density (2.0 mA cm^{–2} at 1.23 V vs RHE). The relation between the wire temperature,

Ti species and defects is reasonable for the evaluation of photocurrent density.

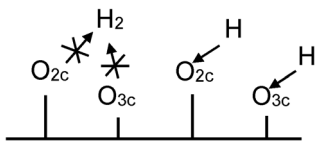
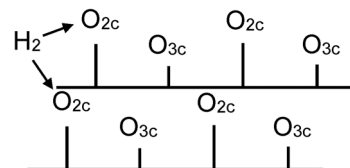
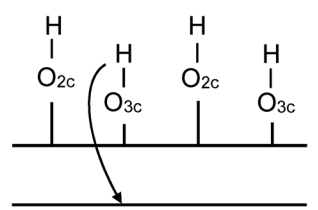
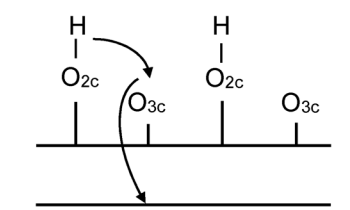
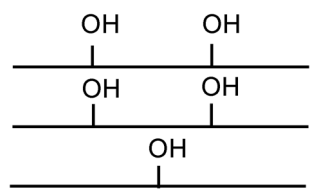
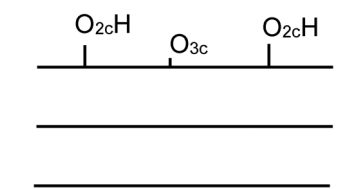
In summary, the interaction between [H] and TiO₂ at different wire temperatures results in different Ti species and defects which are responsible for different PEC activities.

2.5. Comparison of H₂ and [H]-Based Hydrogenation

To better understand the hydrogenation efficiency of HWA, HWA is compared with the conventional molecular hydrogen approaches (Figure S12, Tables S5–S7, Supporting Information). The HWA approach provides a low temperature (265 °C) with low pressure (1 Pa) for TiO₂ treatment, which is close to the low temperature of high-pressure molecular hydrogen treatment (200 °C, 20 bar, 5 days).^[7] However, the hydrogenation efficiency is significantly improved with the treatment time reduced from

5 days to only 20 min via the HWA method. In comparison to the high-temperature hydrogen gas approach (400 °C, 1 bar, 1 h),^[8] HWA treated the samples at a low temperature to avoid the degradation of FTO electrodes and destruction of TiO₂. If we consider the hydrogen flux in both case, about 139 atomic hydrogens hit on the (110) unit cell area whereas $\approx 1.4 \times 10^9$ molecular hydrogens hit on the (110) unit cell area. It is evident that our HWA approach is a more efficient hydrogenation method. Using DFT simulation, we studied the possible formation mechanism of black TiO₂ upon atomic hydrogen treatment in comparison to the molecular one. The gained physical insight confirmed our experimental observations. It indicated that the two hydrogen treatment procedures might provide different pathways of TiO₂ hydrogenation (Table 1). From the thermodynamic point of view, atomic hydrogen is more favorable to be incorporated within the TiO₂ lattice. Low energy barriers for hydrogen adsorption and diffusion into the subsurface region of TiO₂ allow hydrogenation

Table 1. Different formation pathways of disordered shell: [H] versus H₂.

	[H]	H ₂
Hydroxylation	<p>Almost no barrier for adsorption of atomic hydrogen → Low temperature is sufficient H₂ desorption is suppressed due to high energy barrier</p> <p style="text-align: center;">Low T</p> 	<p>High barrier for dissociative adsorption molecular hydrogen → High temperature and flux are needed High surface coverages are not thermodynamically favorable</p> <p style="text-align: center;">High T</p> 
Subsurface diffusion	<p>Lower barrier for subsurface diffusion pathway is O_{3c} → O_{sub} Subsurface diffusion is faster than H₂ and H₂O desorption at low temperatures</p> 	<p>High barrier for subsurface diffusion pathway is O_{2c} → O_{3c} → O_{sub} Subsurface diffusion is very slow</p> 
Subsurface H-doping	<p>Incorporation of H in TiO₂ lattice is thermodynamically favorable up to high concentrations</p> 	<p>Incorporation of H in TiO₂ lattice is not thermodynamically favorable At high temperatures, incorporation becomes even less favorable</p> 
Formation of disordered shell	<p>Formation of disordered shell is thermodynamically favorable through O_{3c} → O_{sub} → H doping in TiO₂ lattice with relatively low barriers <i>Formation pathway:</i> Low temperatures are enough</p>	<p>O_{2c} → O_{3c} → O_{sub} → H doping in TiO₂ is not thermodynamically favorable and kinetically suppressed <i>Different formation pathway:</i> Only H₂O desorption and formation of oxygen vacancies are thermodynamically favorable → High temperatures are needed</p>

at lower temperatures. High concentrations of hydrogen within the subsurface region lead to a weakening of Ti–O bonds and result in the formation of lattice disorder in a shell near the surface. In contrast, high temperatures or pressures typically have to be applied in molecular hydrogen treatments due to the high barriers for dissociative adsorption of molecular hydrogen. Under these conditions, only the desorption of H₂O and the concomitant formation of oxygen vacancies are thermodynamically favorable in order to generate lattice disorder.

3. Conclusions

In summary, we presented a facile, low-temperature and highly efficient method for controllable atomic hydrogenation treatment on TiO₂ nanorods. In an HWA process, the active atomic hydrogen is generated catalytically on the surfaces of heated tungsten wires and is capable to achieve high-quality H–TiO₂ surfaces without introducing side effects on the sensitive H–TiO₂ surface structure. Such a low-temperature process also eliminates the degradation of FTO substrates, which affect the PEC activity. The influences of wire temperatures on the structural, optical, and PEC properties of H–TiO₂ nanorods were systematically characterized. The results demonstrate that atomic hydrogenation leads to the effective and facile formation of a disordered shell on the H–TiO₂ nanorods, which contributes to the narrowed bandgap, increased visible light absorption, and thus a significant improved PEC activity. Besides, DFT simulations reveal that in the case of atomic hydrogen treatment, the formation of a disordered shell is thermodynamically favorable and hydrogen uptake in the subsurface region can proceed through O_{3c} → O_{sub} low-energy-barrier pathway. In the case of molecular hydrogenation, only H₂O desorption and formation of oxygen vacancies are thermodynamically feasible; therefore, high pressure and/or high temperatures are needed. The as-developed HWA method demonstrated its potency for developing a standard hydrogenation method in future and the systematic and fundamental study in this work provide insights into the superior properties of black TiO₂ for a variety of energy applications.

Supporting Information

Supporting Information is available from the Wiley Online Library or from the author.

Acknowledgements

X.D.W. acknowledges the support by the China Scholarship Council (CSC) under the Grand CSC No. 201206950015. The authors would like to thank F. Yu and S.-K. Gurram for technical assistance and thank Prof. W. Shi from Jiangsu University for his scientific comments and suggestion. This work was partially supported by General Research Fund (16237816) from Hong Kong Research Grant Council, ITS/115/18 from Hong Kong Innovation Technology Commission. TEM facilities at CCIT-Universitat de Barcelona are also acknowledged. The authors gratefully acknowledge the computing time granted by the John von Neumann Institute for Computing (NIC) and provided on the supercomputers JURECA and JUWELS at Jülich Supercomputing Centre (JSC).

Conflict of Interest

The authors declare no conflict of interest.

Keywords

atomic hydrogenation, black titania, density functional theory, electron energy loss spectroscopy, photo-electrochemical property, transmission electron microscopy

Received: March 4, 2019

Revised: May 28, 2019

Published online:

- [1] L. Liu, X. Chen, *Chem. Rev.* **2014**, *114*, 9890.
- [2] X. Chen, L. Liu, F. Huang, *Chem. Soc. Rev.* **2015**, *44*, 1861.
- [3] X. Liu, G. Zhu, X. Wang, X. Yuan, T. Lin, F. Huang, *Adv. Energy Mater.* **2016**, *6*, 1600452.
- [4] X. Lü, A. Chen, Y. Luo, P. Lu, Y. Dai, E. Enriquez, P. Dowden, H. Xu, P. G. Kotula, A. K. Azad, D. A. Yarotski, R. P. Prasankumar, A. J. Taylor, J. D. Thompson, Q. Jia, *Nano Lett.* **2016**, *16*, 5751.
- [5] Z. Wang, C. Yang, T. Lin, H. Yin, P. Chen, D. Wan, F. Xu, F. Huang, J. Lin, X. Xie, M. Jiang, *Energy Environ. Sci.* **2013**, *6*, 3007.
- [6] K. Zhang, S. Ravishankar, M. Ma, G. Veerappan, J. Bisquert, F. Fabregat-Santiago, J. H. Park, *Adv. Energy Mater.* **2017**, *7*, 1600923.
- [7] X. Chen, L. Liu, P. Y. Yu, S. S. Mao, *Science* **2011**, *331*, 746.
- [8] G. Wang, H. Wang, Y. Ling, Y. Tang, X. Yang, R. C. Fitzmorris, C. Wang, J. Z. Zhang, Y. Li, *Nano Lett.* **2011**, *11*, 3026.
- [9] Z. Wang, C. Yang, T. Lin, H. Yin, P. Chen, D. Wan, F. Xu, F. Huang, J. Lin, X. Xie, M. Jiang, *Adv. Funct. Mater.* **2013**, *23*, 5444.
- [10] C. Xu, Y. Song, L. Lu, C. Cheng, D. Liu, X. Fang, X. Chen, X. Zhu, D. Li, *Nanoscale Res. Lett.* **2013**, *8*, 391.
- [11] P. Yan, G. Liu, C. Ding, H. Han, J. Shi, Y. Gan, C. Li, *ACS Appl. Mater. Interfaces* **2015**, *7*, 3791.
- [12] G. Zhu, Y. Shan, T. Lin, W. Zhao, J. Xu, Z. Tian, H. Zhang, C. Zheng, F. Huang, *Nanoscale* **2016**, *8*, 4705.
- [13] Y. Xu, C. Zhang, L. Zhang, X. Zhang, H. Yao, J. Shi, *Energy Environ. Sci.* **2016**, *9*, 2410.
- [14] P. M. Kowalski, B. Meyer, D. Marx, *Phys. Rev. B* **2009**, *79*, 115410.
- [15] R. Wang, H. Fan, *Catal. Sci. Technol.* **2017**, *7*, 251.
- [16] W. Karim, C. Spreafico, A. Kleibert, J. Gobrecht, J. VandeVondele, Y. Ekinici, J. A. van Bokhoven, *Nature* **2017**, *541*, 68.
- [17] Y. Du, N. G. Petrik, N. A. Deskins, Z. Wang, M. A. Henderson, G. A. Kimmel, I. Lyubinetsky, *Phys. Chem. Chem. Phys.* **2012**, *14*, 3066.
- [18] X.-L. Yin, M. Calatayud, H. Qiu, Y. Wang, A. Birkner, C. Minot, C. Wöll, *ChemPhysChem* **2008**, *9*, 253.
- [19] G. H. Enevoldsen, H. P. Pinto, A. S. Foster, M. C. R. Jensen, W. A. Hofer, B. Hammer, J. V. Lauritsen, F. Besenbacher, *Phys. Rev. Lett.* **2009**, *102*, 136103.
- [20] G. H. Enevoldsen, H. P. Pinto, A. S. Foster, M. C. R. Jensen, W. A. Hofer, B. Hammer, J. V. Lauritsen, F. Besenbacher, *Phys. Rev. Lett.* **2010**, *104*, 119604.
- [21] M. M. Islam, M. Calatayud, G. Pacchioni, *J. Phys. Chem. C* **2011**, *115*, 6809.
- [22] M. V. Koudriachova, S. W. de Leeuw, N. M. Harrison, *Phys. Rev. B* **2004**, *70*, 165421.
- [23] I. Langmuir, *J. Am. Chem. Soc.* **1912**, *34*, 860.
- [24] K. Abe, M. Ida, A. Izumi, S. Terashima, T. Sudo, Y. Watanabe, Y. Fukuda, *Thin Solid Films* **2009**, *517*, 3449.

- [25] C. Fàbrega, D. Monllor-Satoca, S. Ampudia, A. Parra, T. Andreu, J. R. Morante, *J. Phys. Chem. C* **2013**, *117*, 20517.
- [26] S. Xie, M. Li, W. Wei, T. Zhai, P. Fang, R. Qiu, X. Lu, Y. Tong, *Nano Energy* **2014**, *10*, 313.
- [27] Y. Qiu, S.-F. Leung, Q. Zhang, B. Hua, Q. Lin, Z. Wei, K.-H. Tsui, Y. Zhang, S. Yang, Z. Fan, *Nano Lett.* **2014**, *14*, 2123.
- [28] Y. Qiu, S.-F. Leung, Z. Wei, Q. Lin, X. Zheng, Y. Zhang, Z. Fan, S. Yang, *J. Phys. Chem. C* **2014**, *118*, 22465.
- [29] L. Caccamo, J. Hartmann, C. Fàbrega, S. Estradé, G. Lilienkamp, J. D. Prades, M. W. G. Hoffmann, J. Ledig, A. Wagner, X. Wang, L. Lopez-Conesa, F. Peiró, J. M. Rebled, H.-H. Wehmann, W. Daum, H. Shen, A. Waag, *ACS Appl. Mater. Interfaces* **2014**, *6*, 2235.
- [30] Z. Fan, H. Razavi, J.-w. Do, A. Moriwaki, O. Ergen, Y.-L. Chueh, P. W. Leu, J. C. Ho, T. Takahashi, L. A. Reichertz, S. Neale, K. Yu, M. Wu, J. W. Ager, A. Javey, *Nat. Mater.* **2009**, *8*, 648.
- [31] Z. Fan, R. Kapadia, P. W. Leu, X. Zhang, Y.-L. Chueh, K. Takei, K. Yu, A. Jamshidi, A. A. Rathore, D. J. Ruebusch, M. Wu, A. Javey, *Nano Lett.* **2010**, *10*, 3823.
- [32] M. Yu, Y.-Z. Long, B. Sun, Z. Fan, *Nanoscale* **2012**, *4*, 2783.
- [33] S.-F. Leung, Q. Zhang, M. M. Tavakoli, J. He, X. Mo, Z. Fan, *Small* **2016**, *12*, 2536.
- [34] J. Li, Y. Qiu, Z. Wei, Q. Lin, Q. Zhang, K. Yan, H. Chen, S. Xiao, Z. Fan, S. Yang, *Energy Environ. Sci.* **2014**, *7*, 3651.
- [35] *Photoelectrochemical Water Splitting: Materials, Processes and Architectures* (Eds: H. J. Lewerenz, L. Peter), Royal Society of Chemistry, Cambridge, UK **2013**.
- [36] C. Yang, Z. Wang, T. Lin, H. Yin, X. Lü, D. Wan, T. Xu, C. Zheng, J. Lin, F. Huang, X. Xie, M. Jiang, *J. Am. Chem. Soc.* **2013**, *135*, 17831.
- [37] T. Leshuk, R. Parviz, P. Everett, H. Krishnakumar, R. A. Varin, F. Gu, *ACS Appl. Mater. Interfaces* **2013**, *5*, 1892.
- [38] L. Liu, P. Y. Yu, X. Chen, S. S. Mao, D. Z. Shen, *Phys. Rev. Lett.* **2013**, *111*, 065505.
- [39] D. Ugur, A. J. Storm, R. Verberk, J. C. Brouwer, W. G. Sloof, *J. Vac. Sci. Technol., A* **2012**, *30*, 031603.